iPAT Applications in Clinical Routine and Beyond: Imaging from Head to Toe

Olaf Dietrich, PhD; Stefan O. Schoenberg, MD

Department of Clinical Radiology – Großhadern (Chairman: Maximilian F. Reiser, MD),
Ludwig-Maximilians-University of Munich, Germany

Corresponding author:
Olaf Dietrich, PhD
Ludwig-Maximilians-University of Munich
Department of Clinical Radiology – Großhadern
Marchioninistraße 15, 81377 Munich, Germany
Phone: +49 89 7095-4622
Fax: +49 89 7095-4627
E-mail: od@dtrx.net

Introduction

With the release of Numaris 4 version MR2002B an important new feature has become available for routine examination: *integrated Parallel Acquisition Techniques* (iPAT). The general idea behind iPAT is to acquire image data simultaneously by two or more receiver coils with different spatial sensitivities. Initially, this technique was motivated by the wish to accelerate image acquisition without reducing the spatial resolution of the image. However, it turned out that iPAT provides several other advantages depending on the application.

Technical Background

Acquisition of MR images works by subsequently acquiring phase-encoded lines in k-space. These lines of data are finally transformed into the image slice (or slab in the case of 3D acquisitions) by a mathematical process called Fourier transform. An important property of data in k-space is that the density or "distance" of the lines in k-space corresponds inversely to the field of view (FOV) of the final image whereas the data range in k-space corresponds to the spatial resolution of the image. I.e. reducing the line sampling density by a factor of 2 (by not acquiring every other line) leads to an image with half the FOV in phase-encoding direction in comparison with the original image. In this case, the acquisition time is also reduced by a factor of 2 as is well known from using rectangular FOVs. iPAT methods use exactly this effect to accelerate image acquisition, but without decreasing the FOV due to a special iPAT image reconstruction. Using the complementary data from the different receiver coils, the "missing" lines in k-space can be calculated during image reconstruction.

There are two groups of iPAT algorithms: algorithms that explicitly calculate missing k-space lines before Fourier transforming the data, and algorithms that first reconstruct images with reduced FOV for all receiver coil elements and then merge these different images into one with full FOV. Numaris 4 MR2002B provides both types of algorithms: GeneRalized Auto-calibrating Partially Parallel Acquisition (GRAPPA) is an algorithm of the first type [1]; it is based on another well-known algorithm of the same class called Simultaneous Acquisition of Spatial Harmonics (SMASH) [2]. The best-known algorithm of the second type has been called SENSitivity-Encoded (SENSE) MRI [3] and a modified SENSE algorithm called mSENSE is available under MR2002B. It depends on the specific application (e.g., on the anatomical region and pulse sequence) which of these two iPAT algorithm will yield better image quality.

Both GRAPPA and mSENSE algorithm require some additional information about the spatial coil sensitivities, i.e. which part of the FOV is covered by each coil element. This information can be acquired as separate extra scan with low resolution or, typical for the GRAPPA and mSENSE algorithm, by additionally acquiring some of the missing data lines in the center of k-space (so-called reference lines) integrated into the acquisition. Total imaging time will be slightly increased due to the read-out of the reference lines and in certain situation it might be preferable to use a pulse sequence with external reference scan.

Generally, the signal-to-noise ratio (SNR) in iPAT images is decreased compared to acquisitions with the full k-space data. This is the same effect as in conventional imaging with rectangular FOV: acquiring fewer lines in k-space decreases the SNR of the image. Additionally, iPAT images suffer an SNR loss due to the special reconstruction scheme: this effect depends on the efficacy of the geometry of coil distribution and is described by the so-called "geometry factor" *g* [3].

Advantages and Disadvantages of iPAT

The obvious advantage of iPAT is the acceleration of imaging due to the reduced number of phase-encoding lines to be acquired. With an acceleration factor (or iPAT factor) of 2, i.e. acquisition of only every second line in k-space, the imaging time is reduced by 40 % to 50 % depending on the number of reference lines. This can be used to decrease the overall examination time and thus improve the patient throughput and examination efficacy. Alternatively, the spatial image resolution can be improved in an iPAT scan compared to a conventional scan of the same duration. Both shorter scan times and higher resolution are especially important in breath-hold imaging: either breath-hold times can be shortened or the spatial resolution can be improved without prolonging the breath-hold time.

Another important iPAT application is dynamic imaging like measurements of perfusion or cardiac function because image acceleration allows for a higher temporal resolution. However, as mentioned above the resulting SNR will be decreased compared to non-iPAT acquisitions; hence, iPAT is especially useful for high-SNR applications like contrast-enhanced angiography.

Using iPAT to acquire more averages in the same total scan time can improve image quality, particularly in anatomical areas that are prone to motion artifacts. iPAT imaging is less sensitive to motion, because every single acquisition is shorter than in a conventional sequence. By averaging image data, the iPAT-related SNR loss is almost compensated and remaining motion artifacts are further reduced.

Single-shot pulse sequences like echo-planar imaging (EPI) or half-Fourier acquired single-shot turbo spin echo (HASTE) often suffer from image artifacts due to their long echo trains. EPI is especially sensitive to susceptibility artifacts, whereas HASTE images often appear blurred due to the T2-related signal decay during the readout of the echo train. Both problems can be reduced by applying iPAT to shorten the length of the echo train without loss of spatial resolution. In contrast to other pulse sequences, single-shot methods can even gain SNR due to iPAT because late echoes with relatively low signal intensity that are acquired in conventional sequences are not contained in the shortened iPAT echo train.

In conclusion, iPAT can be advantageous in very different applications with very different ways of using iPAT. This is demonstrated in the following sections with examples ranging from clinical routine imaging to advanced study protocols. Imaging in all presented applications is performed on a 1.5 T MAGNETOM Sonata Maestro Class system. Standard Numaris sequences are used in most cases; however, some applications require sequences from special "work in progress" (WIP) packages by Siemens Medical Solutions.

Diffusion Tensor Imaging

Diffusion tensor imaging (DTI) is an advanced MR imaging technique for measuring the strength, anisotropy, and direction of water diffusion in tissue. The term "water diffusion" refers to the property of all water molecules to move stochastically due to their thermal energy (Brownian motion). The extent of this motion is restricted by tissue properties, particularly by the cellular microstructure and the spatial orientation of cells. Especially in fiber structures like muscle tissue or the cerebral white matter, molecular motion is restricted by cell membranes or myelin sheaths, and molecules move preferably parallel to the fiber direction whereas diffusion orthogonal to the fiber direction is decreased. Thus, the resulting water diffusion is anisotropic. Information about the diffusion

strength (apparent diffusion coefficient, ADC), diffusion anisotropy, and diffusion direction are contained in the so-called diffusion tensor, a mathematical object (symmetric 3×3 matrix) consisting of 6 independent numbers.

The most common pulse sequences to measure the diffusion tensor are diffusion-weighted EPI sequences with diffusion gradients applied in at least six different directions [4, 5]. Single-shot EPI sequences have the advantage that imaging is fast (about 100 ms/image) and thus very insensitive to motion. However, EPI sequences are very prone to susceptibility artifacts manifesting as distortions in the frontal brain and the cranial base. This disadvantage can be overcome by using iPAT sequences to shorten the length of the EPI gradient echo train. Hence, we use a spin echo EPI diffusion sequence with GRAPPA reconstruction, an acceleration factor of 2, and 24 reference lines for DTI examinations. A dedicated iPAT head coil consisting of 8 surface coil elements (Fig. 1) provides the required number of receiver channels.

Figure 1 8-channel phased-array head coil for acquisition of iPAT data. 8 surface coil elements are located cylindrically around the AP axis; the inner diameter of the coil is 24 cm.

Acquisition with the 8-channel head coil results in images with an improved SNR compared to the standard quadrature head coil (Fig. 2). This can be explained by the smaller diameter of the 8-channel head coil (24 cm vs. 26 cm) and the reduced coil size in cranio-caudal direction. Images were acquired with a 128×128 matrix in 36 slices, 230×230 mm^2 FOV, phase-encoding in anterior-posterior direction, a slice thickness of 3.6 mm, 10 averages, and an iPAT factor of 2 (24 reference lines); the echo time was 71 ms and the repeat time 6000 ms. DTI with iPAT displays less distortion artifacts than DTI with conventional EPI sequences (Fig. 3). Evaluating the diffusion-weighted images, parameter maps with the mean ADC, the diffusion anisotropy, and the main direction of diffusion can be calculated (Fig. 4). Although an N/2 artifact in phase-encoding direction (anterior-posterior) is visible in some of the original EPI images, this artifact seems not to influence the calculated parameter maps. An additional advantage of iPAT imaging is the reduced duration of the readout that allows for the acquisition of an increased number of slices within the given repetition time (TR) compared to conventional sequences; e.g., 38 slices without iPAT vs. 50 slices with iPAT given a TR of 6000 ms.

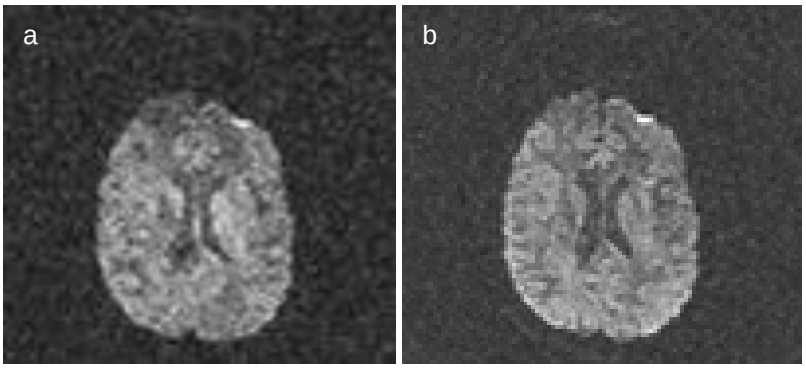

Figure 2 Comparison of SNR with standard head coil (a) and 8-channel head coil (b). Both images are acquired with identical sequence parameters (diffusion-weighted EPI sequence, $b = 1000$ s/mm^2, no averaging) and without iPAT.

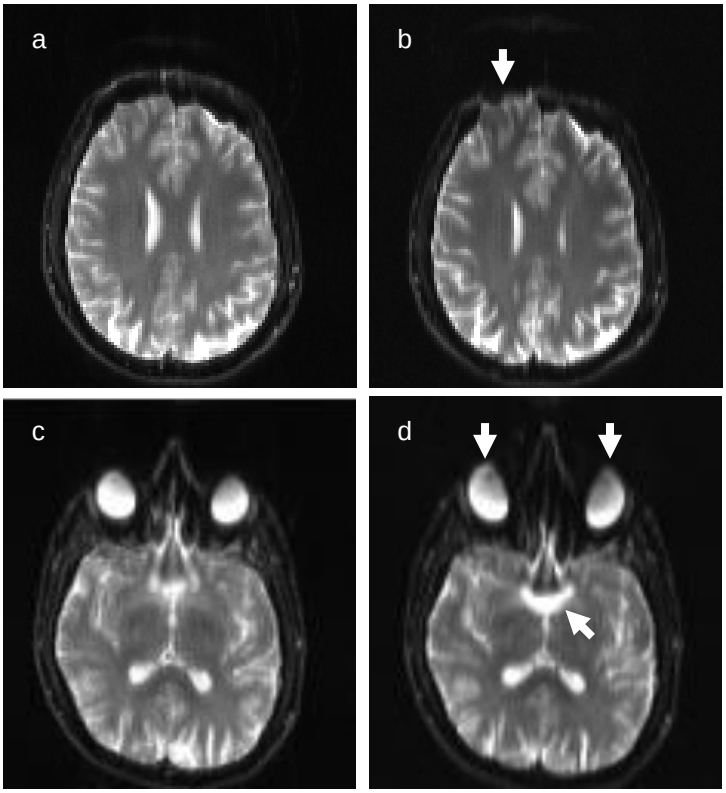

Figure 3 Comparison of spin echo EPI images in two slices with (a, c) and without (b, d) iPAT (GRAPPA algorithm). Some obvious susceptibility artifacts are marked with arrows in (b) and (d).

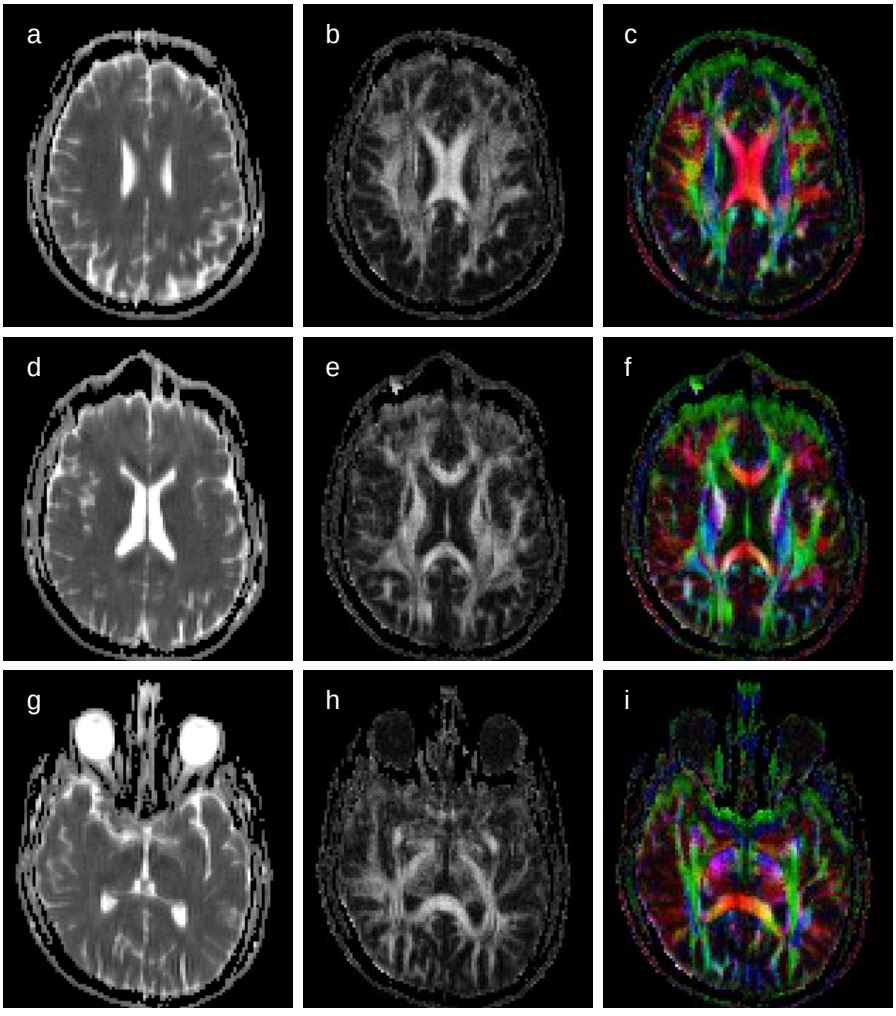

Figure 4 Examples of DTI evaluation from diffusion-weighted iPAT images: ADC map (a, d, g) with diffusion coefficients from 0 (black) to 2.5×10^{-3} mm^2/s (white); fractional anisotropy (b, e, h) from 0 (black) to 1 (white); color-coded main diffusion direction (c, f, i), left-right: red, anterior-posterior: green, cranio-caudal (blue). Note especially the high anisotropy and left-right diffusion direction in the corpus callosum.

Larynx Imaging

Magnetic resonance imaging of the larynx is difficult due to tissue motion caused by swallowing and respiration [6]. Generally, MR pulse sequences with long acquisition times are more sensitive to motion than fast imaging sequences or even single-shot sequences. Therefore, MRI of the larynx at conventional speed often leads to images with excessive motion artifacts.

Since moving organs like the larynx can be more clearly visualized by reducing the image acquisition time, iPAT sequences can reduce the sensitivity to motion artifacts by accelerating image acquisition while maintaining the same image resolution. Thus, we use T1-weighted and T2-weighted iPAT sequences for routine larynx imaging, e.g. in patients suffering from suspected laryngeal carcinoma. A pair of dedicated iPAT surface coil systems with 2×6 coil elements is arranged around head and neck of the patient. To compensate for the iPAT intrinsic SNR loss, we increase the number of acquisitions to 5 (T1-weighted gradient echo sequence with TR/TE = 176 ms/4.8 ms, 24 iPAT reference lines) and 3 (T2-weighted TSE sequence with TR/TE = 3970 ms/89 ms, echo train length 15, 45 iPAT reference lines). Both sequences have a 512×384 matrix, a FOV of 300×281.3 mm^2 and a slice thickness of 3.5 mm. The GRAPPA algorithm is used for iPAT reconstruction.

The acquired images show a better delineation of tumor extent and less motion artifacts than MRI using non-iPAT techniques, thus allowing accurate diagnosis of laryngeal carcinoma (Fig. 5). In our experience, MRI with iPAT using a flexible 12-element phased-array coil is suitable for reliable diagnosis when laryngeal carcinoma is suspected. Generally, in imaging moving tissue it appears preferable to acquire more averages with reduced imaging time using iPAT and thus gain images with identical resolution and comparable SNR but less motion artifacts than in conventional non-iPAT imaging.

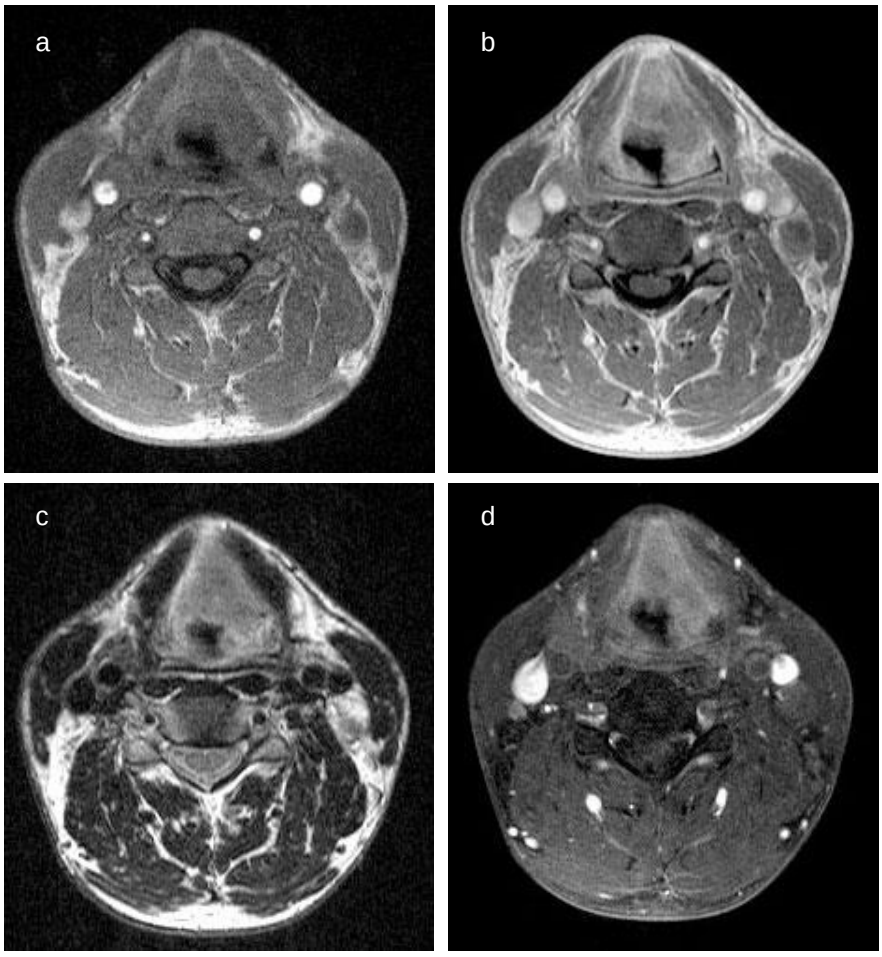

Figure 5 Axial MRI scan through the supraglottic larynx, all images show the same scan position. The images demonstrate a large supraglottic tumor infiltrating the preepiglottic space, the left paraglottic space and the left aryepiglottic fold. (a) T1-weighted image showing muscle-isointense tumor. (b) T1-weighted image demonstrating contrast-enhancement of the tumor. (c) T2-weighted axial image showing slightly hyperintense tumor tissue. (d) T1-weighted fatsat image demonstrating contrast enhancement of the tumor. Spinocellular carcinoma was found at surgery.

Lung Imaging

MR Screening of Infiltrates

Radiological lung screening is typically performed either by conventional x-ray (CXR) examination or by high-resolution computed tomography (HR-CT) of the thorax and therefore exposes patients to a considerable amount of radiation, particularly after repeated examinations. This radiation dose could be reduced by using MRI as screening modality instead of x-ray based methods. Unfortunately, MRI of the lung is still a technical challenge because of the very low proton density of the lung tissue and the strong variation of susceptibility leading to very short T2* relaxation times. Both factors together are the reason for very low MR signal intensities from lung parenchyma and hence for a low SNR. A further difficulty in lung MRI is tissue motion because of respiration and cardiac motion.

The introduction of iPAT opened new possibilities to lung imaging with T2-weighted HASTE sequences. The main disadvantage of conventional HASTE sequences is the blurring of images caused by the long echo train and the T2-related signal decay during its readout; this effect severely limited the actual maximum image resolution [7]. By using iPAT, the echo train can be reduced to half of its original length and thus blurring artifacts are reduced. Since late echoes with low signal intensity are not acquired, SNR can even improve compared to non-iPAT sequences. Additionally, the image acquisition is accelerated such that more slices can be acquired during one breath-hold period.

To evaluate the use of iPAT HASTE sequences for lung screening, we compared HR-CT and MR images in immunosuppressed patients with symptoms of pneumonia but normal or unspecific CXR. After comparing iPAT images reconstructed with the GRAPPA and mSENSE algorithm (Fig. 6), we decided to use the GRAPPA algorithm because of the occurrence of reconstruction artifacts in the image center of the mSENSE images. Coronal slices of the lung are acquired with a FOV of 400×400 mm^2 and a resolution of 320×320 pixels; axial slices with a FOV of 400×320 mm^2 and a 320×256 matrix. The slice thickness is 8 mm and the TE is 27 ms in both sequences. To reduce the echo train length as far as possible, a Siemens WIP sequence with external iPAT reference scan was used; the sequence acquires the reference lines immediately before the actual image acquisition within the same breath-hold. Examples of the findings are shown in Fig. 7–10.

We found that lung MRI with iPAT HASTE sequences is nearly as good as HR-CT for the detection of pulmonary infiltrates with only few false-negative and false-positive cases such that MRI can be recommended especially as a follow-up tool after initial HR-CT diagnosis.

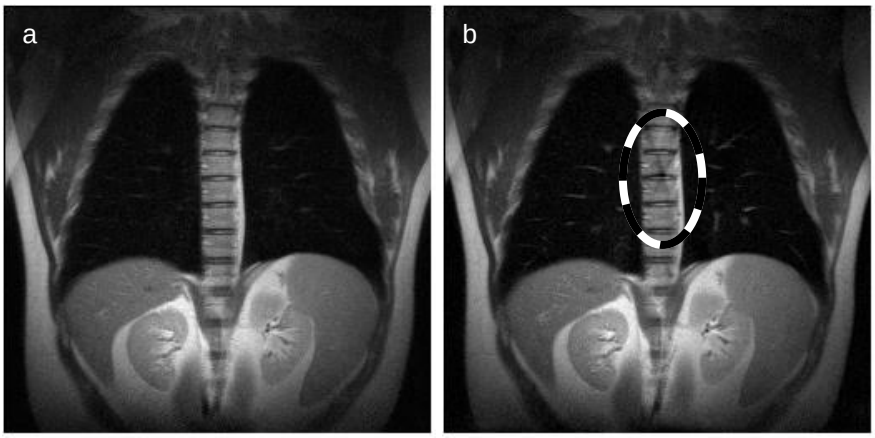

Figure 6 iPAT HASTE images of a healthy volunteer reconstructed with GRAPPA (a) and mSENSE (b) algorithm. Note the reconstruction artifacts superposing the spine in (b).

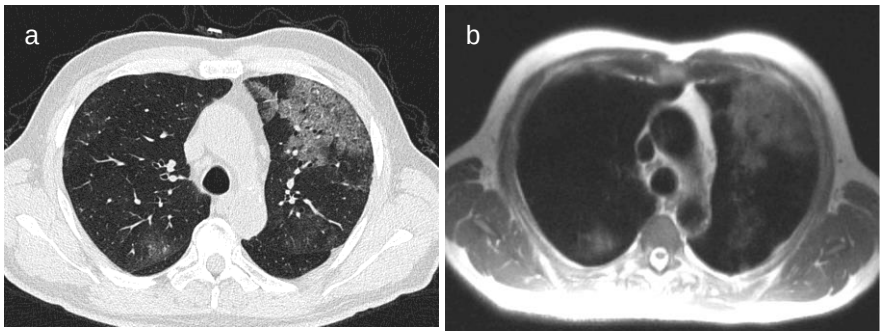

Figure 7 Ground glass infiltrate in immunosuppressed patient. Multidetector HR-CT (a) and iPAT HASTE MRI (b).

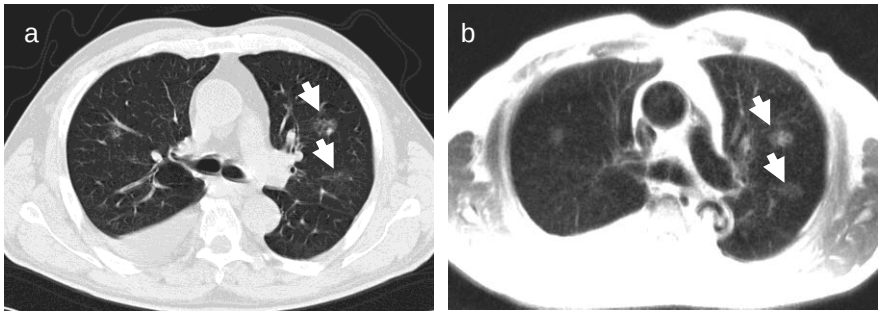

Figure 8 Small irregular infiltrates in immunosuppressed patient. Multi-detector HR-CT (a) and iPAT HASTE MRI (b).

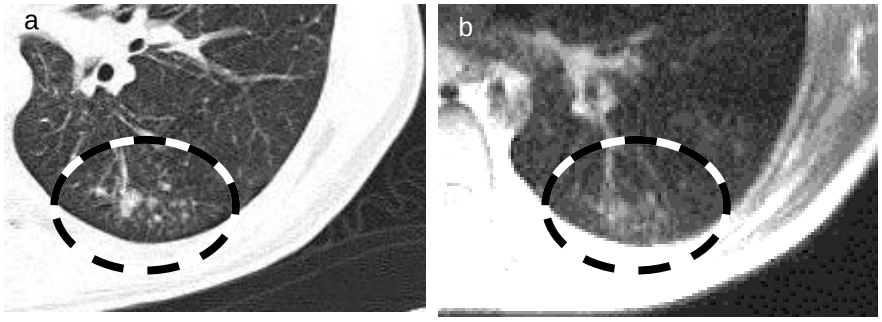

Figure 9 Discrete atypical infiltrates in immunosuppressed patient. Multi-detector HR-CT (a) and iPAT HASTE MRI (b).

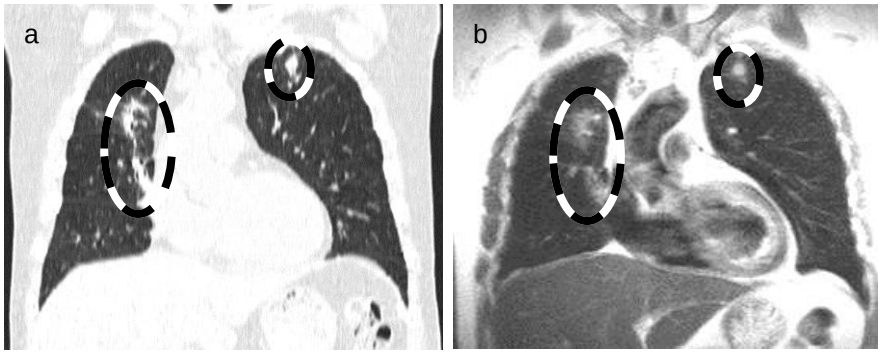

Figure 10 Discrete atypical infiltrates in immunosuppressed patient. Multi-detector HR-CT (a) and iPAT HASTE MRI (b).

MR Angiography and Perfusion Imaging

Contrast-enhanced vascular lung MRI requires a good spatial resolution and—especially in the case of perfusion imaging—also a good temporal resolution. Both are limited rather by the breath-hold duration for the patient than by SNR considerations due to the high-contrast situation in contrast-enhanced MRI. Experiences on MR perfusion imaging of the lung are still limited and various approaches like conventional FLASH and HASTE sequences or flow-sensitive inversion recovery techniques are being used [8–10]. However, using iPAT techniques, both temporal and spatial resolution can be significantly increased compared with conventional imaging.

Therefore, we added iPAT FLASH sequences to our protocol for 3D contrast-enhanced MR angiography (MRA) and MR perfusion imaging of patients with primary and secondary pulmonary arterial hypertension. Using GRAPPA with the dedicated 12-element iPAT coil, a temporal resolution of 1.2 seconds per phase is possible for dynamic perfusion imaging, acquiring 25 dynamic phases in 30 seconds; the image resolution is 1.5×3.0×4.0 mm^3 acquired with a 256×128 matrix in 24 slices. High resolution angiograms can be acquired with a 512 matrix (0.8×1.0×1.6 mm^3 voxel size) in 20 seconds breath-hold time. For both dynamic perfusion and high-resolution angiography, an iPAT acceleration factor of 2 is used with 24 additionally acquired reference lines.

Image examples of these sequences are shown in Fig. 11 and 12. Using the parallel acquisition technique, excellent visualization of subsegmental vessels is possible in the angiographic images. Time-resolved perfusion imaging allows a reliable detection of small segmental and subsegmental perfusion defects. Using non-iPAT methods, visualization of perfusion defects and intravascular thrombi is generally possible as well, although with lower temporal and spatial resolution than using iPAT methods. In conclusion, we could substantially improve the temporal resolution as well as the spatial resolution by using iPAT.

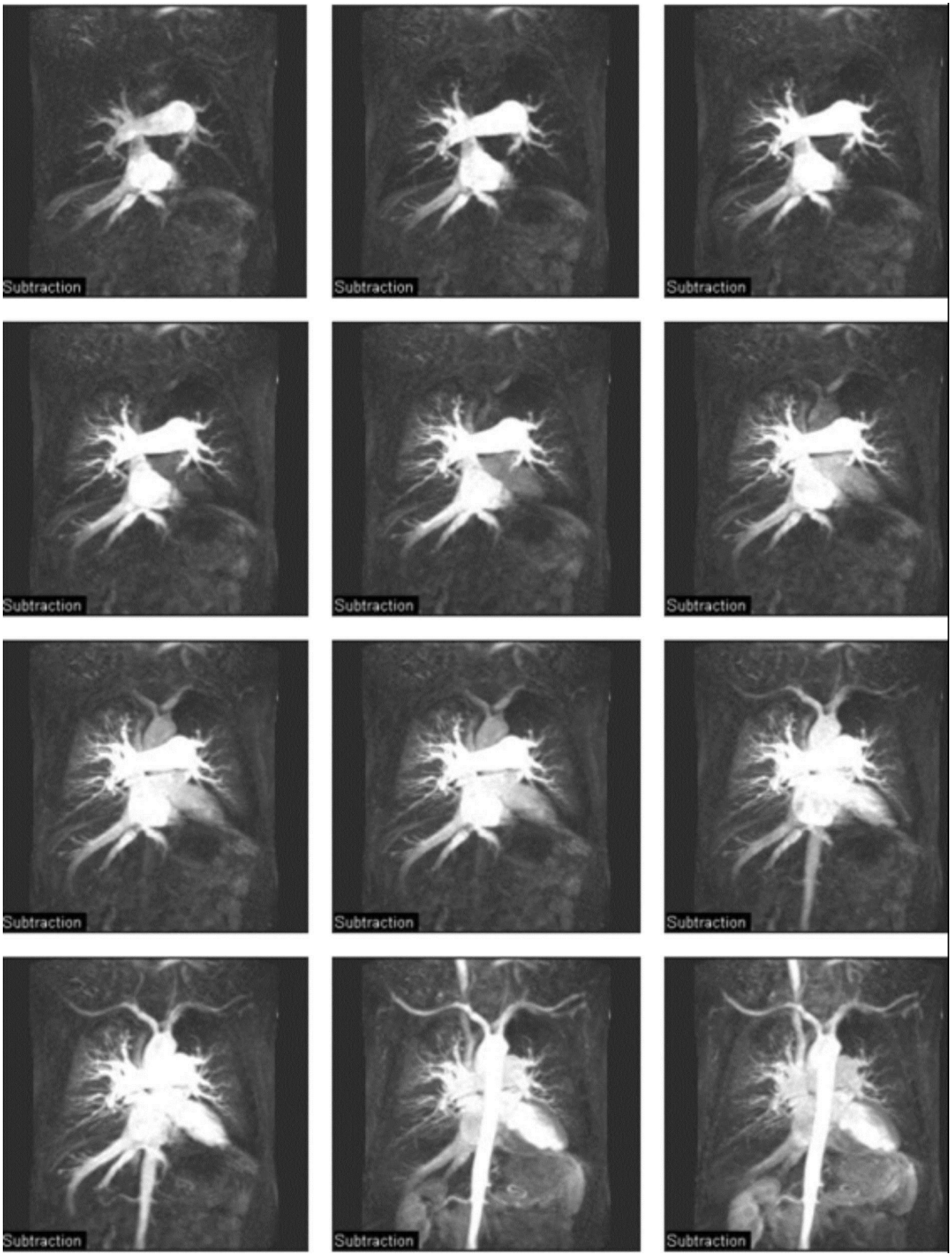

Figure 11 Dynamic pulmonary perfusion imaging using iPAT to acquire a slab of 24 images each 1.2 seconds. Perfusion defects are shown in the left upper lobe and right lower lobe.

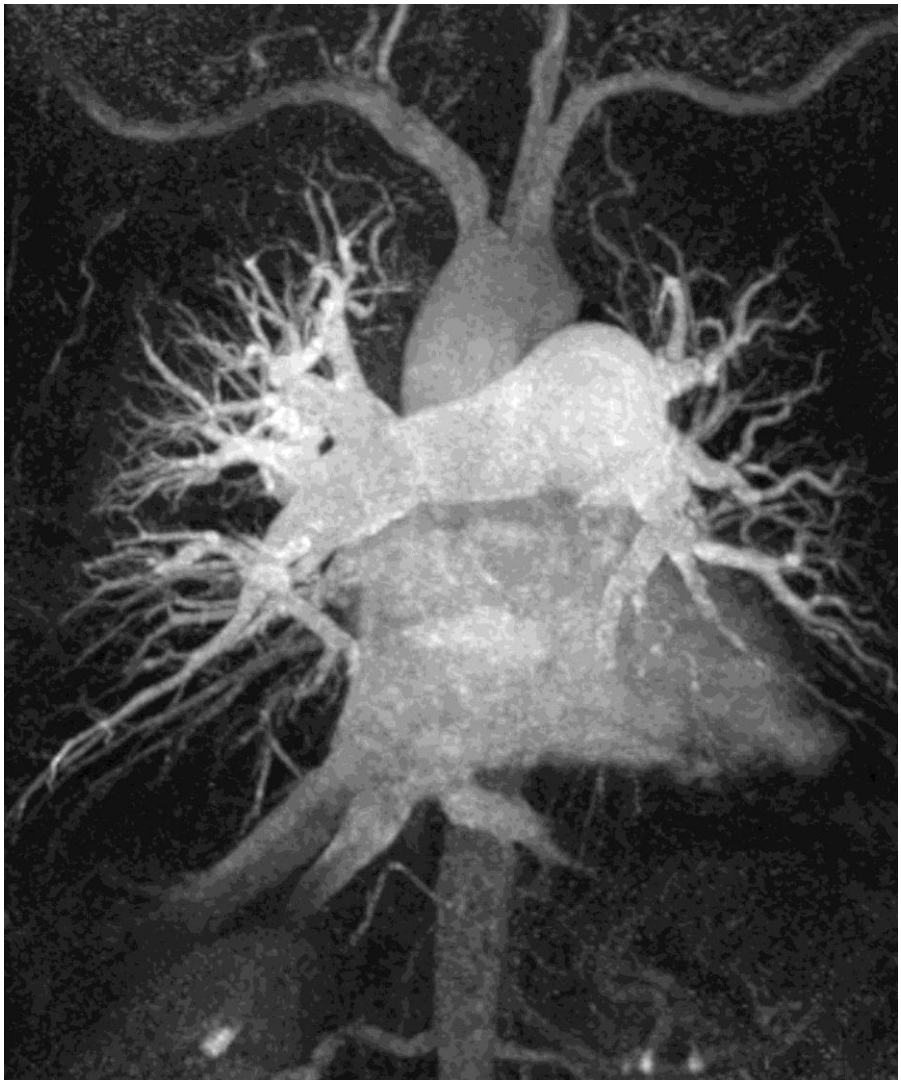

Figure 12 Example of an iPAT high-resolution pulmonary MR angiography of the same patient as in Fig. 11. A significant reduction of arterial enhancement can be demonstrated in the left upper lobe and right lower lobe due to central thromboembolic occlusions.

Functional Cardiac Imaging

Global and Regional Cardiac Function

Cardiac magnetic resonance imaging has been extensively used in assessment of global and regional myocardial function. There is no doubt that MRI represents the current standard of reference. Although dataset acquisition can be performed in virtually any plane, the calculation of functional parameters is most commonly based on a stack of slices in double oblique short axis orientation. To allow for high spatial as well as high temporal resolution, the current sequence techniques acquire a single-slice cine data set each breath-hold. Although innovations of recent years allowed for a speed up of techniques, a completion of a standardized functional study still takes about 10–15 minutes including patient recovery periods. Real-time imaging techniques using steady-state free precession (SSFP) sequences such as TrueFISP, allow for a major speed up in data acquisition due to the completion of a short axis dataset within a single breath-hold [11, 12]. However, this comes along with a restriction in spatial and temporal resolution. And in terms of volumetric accuracy, temporal resolution is by far more crucial than spatial resolution as recently shown by Miller and co-workers [13]. The current recommendation for functional cardiac imaging requests a temporal resolution of 50 ms or even better.

iPAT allows meeting this criterion when implemented in conjunction with real-time TrueFISP. Compared to previous studies performed by Barkhausen and Lee [11, 12], the temporal resolution that can be achieved is in the order of 45–50 ms. And as most recently shown, this improvement in temporal resolution now leads to an accuracy of results comparable to that of segmented TrueFISP [14] (Fig. 13–16); the iPAT images are acquired with an acceleration factor of 2 and 12 reference lines. So iPAT allows for dramatic time savings in cardiac function analysis without losing accuracy of volumetric results. It even allows for a multiplanar data acquisition within a single breath-hold.

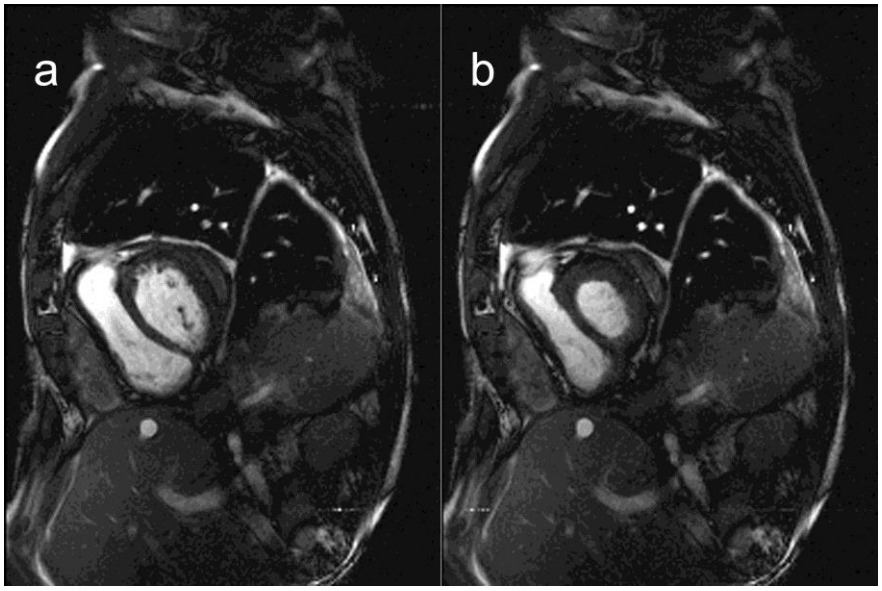

Figure 13 Short axis view of a male patient with impaired right ventricular function due to pericardial disease. Images acquired with a segmented TrueFISP technique showing diastole (a) and systole (b).

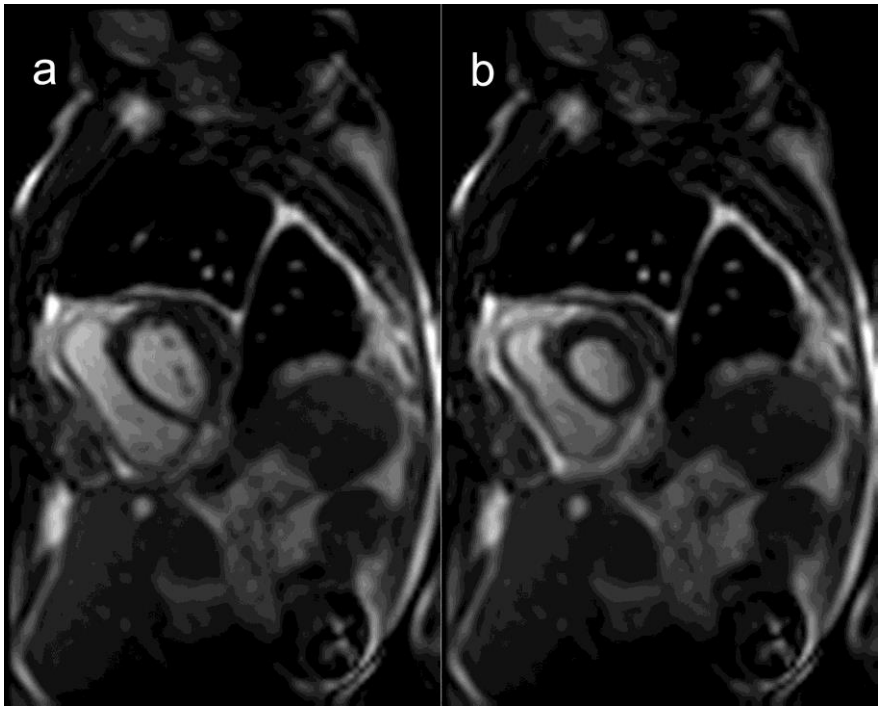

Figure 14 A single slice of the multi-slice iPAT real-time cine data set at exactly the same slice position as in Fig. 13. Comparable time points in (a) diastole and (b) systole.

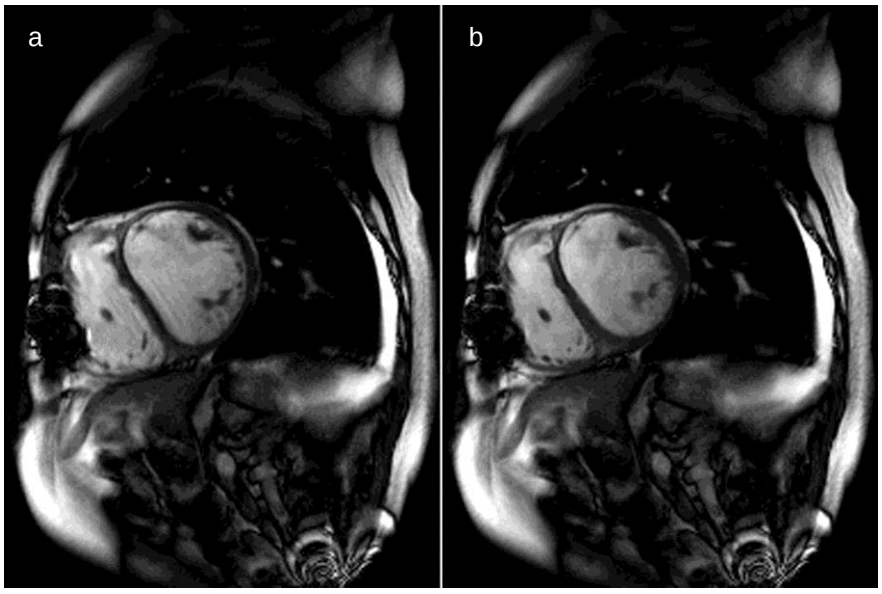

Figure 15 Patient after myocardial infarction with ischemic dilatating cardiomyopathy. Diastolic (a) and systolic (b) images acquired with segmented TrueFISP show almost no change in ventricular shape (ejection fraction < 25 %).

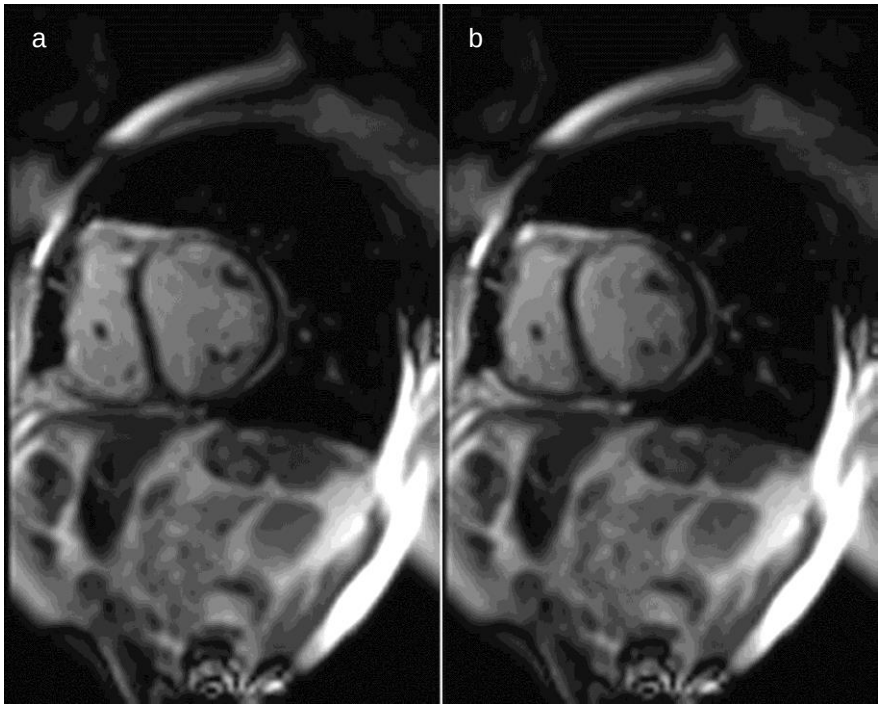

Figure 16 Comparison to Fig. 15 at identical slice position. iPAT real-time TrueFISP shows the same marked thinning of the anterior wall without change within diastole (a) and diastole (b).

Based on experiences and comparisons, the GRAPPA reconstruction shows a more robust image quality in cardiac MRI than mSENSE [1]. Due to the higher sensitivity of SENSE-related methods to folding artifacts, these techniques seem to be less useful in cardiac imaging because of the necessary larger FOV that leads either to an additional loss of spatial resolution or to loss of acquisition time when more phase-encoding lines are acquired. Apart from the use of iPAT with real-time techniques it also allows for a further improvement of spatial or temporal resolution in segmented single-slice acquisitions compared to standard techniques (Fig. 17). In general, when using cine TrueFISP techniques the loss in SNR due to iPAT is almost negligible.

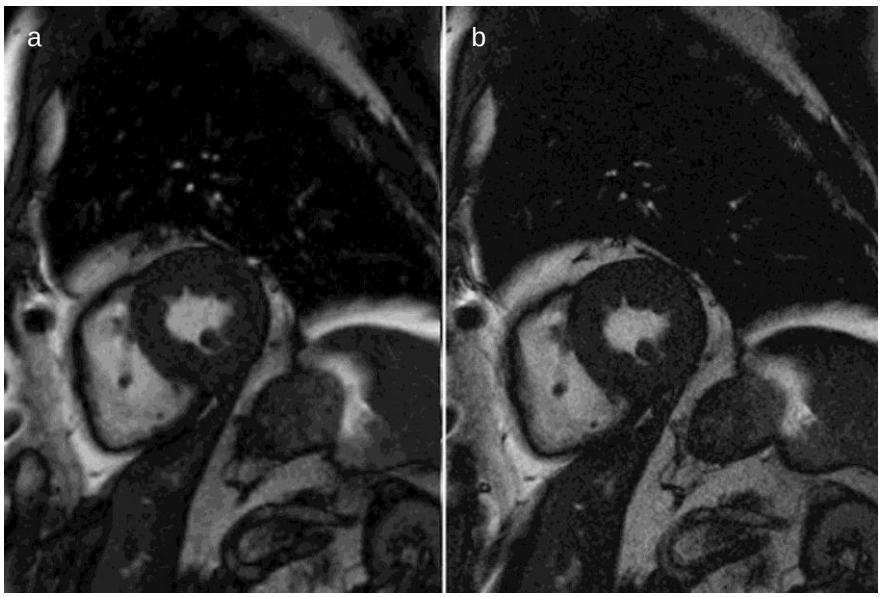

Figure 17 Combination of segmented cine TrueFISP with iPAT. In comparison to standard techniques (a; pixel size 1.5×1.5 mm^2), the use of iPAT allows for a marked increase of spatial resolution (b; pixel size 1×1 mm^2).

Myocardial Perfusion Imaging

Myocardial perfusion imaging is a promising and rapidly increasing field in cardiac MRI. The rapid development of scanner hardware allows also for an improvement in sequence technologies which has been of a major benefit in techniques that require an ultra-fast data acquisition such as myocardial perfusion imaging. MR perfusion imaging has intrinsic benefits compared to routinely used techniques of nuclear medicine such as single photon emission computed tomography (SPECT) imaging or even positron emission tomography (PET) which represents the current gold standard in clinical perfusion imaging. Besides the higher spatial resolution and lack of radiation exposure, myocardial MR perfusion imaging has no attenuation problem related to anatomical limitations.

However, with the use of magnetization-prepared TurboFLASH techniques (e.g. saturation recovery TurboFLASH) the SNR has come to a limit (Fig. 18). Therefore a combination with iPAT techniques seems to be of less benefit, as a further loss in SNR comes along. Newly developed techniques for myocardial perfusion imaging based on SSFP techniques are currently under investigation [15]. In comparison with TurboFLASH techniques, these sequences (available as Siemens WIP package) show a considerable higher intrinsic SNR therefore allowing for a minimal to moderate loss of SNR when combined with iPAT (Fig. 19).

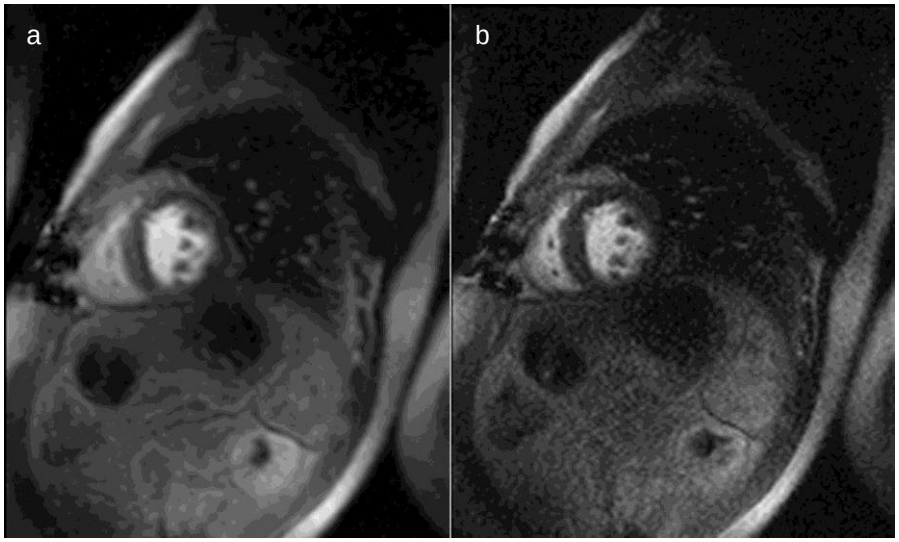

Figure 18 Images of MR perfusion data sets using a saturation recovery TurboFLASH technique. Comparison of a non-iPAT TurboFLASH technique (a) with an iPAT (GRAPPA) TurboFLASH technique (b). There is considerable more noise within the iPAT image which hampers depiction of perfusion abnormalities based on the low SNR.

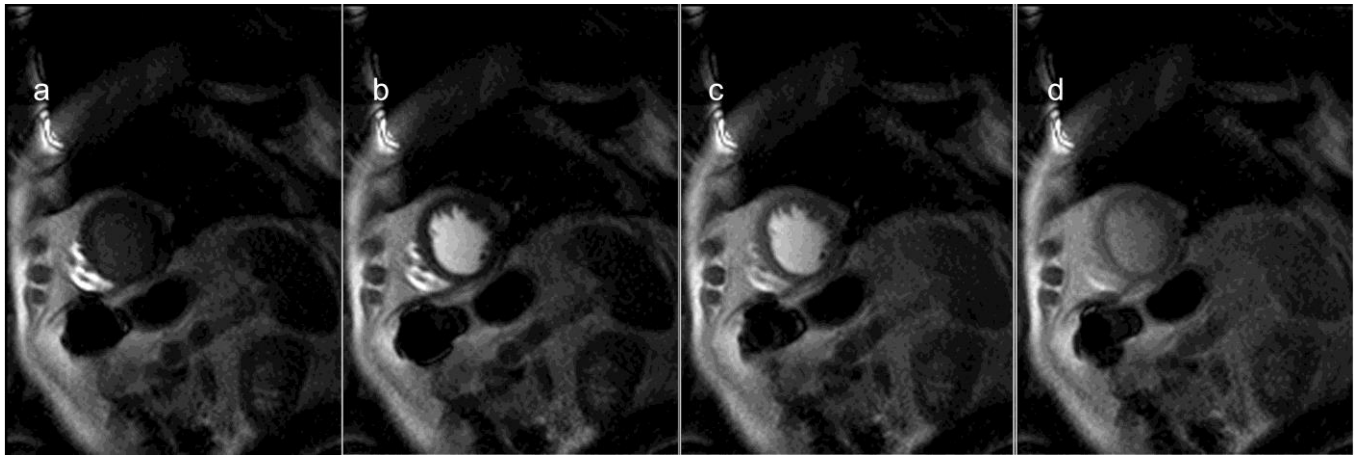

Figure 19 Saturation recovery TrueFISP perfusion images combined with iPAT (GRAPPA) and a high in-plane resolution of 2.1×2.1 mm^2. In contrast to saturation recovery TurboFLASH, the spatial resolution is still high enough to follow signal dynamics.

Liver Imaging

MR liver imaging is most severely restricted by respiratory movement. Therefore, image quality was considerably improved with the introduction of T2-weighted turbo spin echo (TSE) and single-shot sequences. With these techniques, breath-hold examinations of the liver became possible, which most authors consider superior to conventional spin echo sequences [16–18]. Generally, a maximum breath-hold time of about 20 seconds, tolerable even for patients in bad health condition, is a limiting parameter for all sequences used for liver imaging.

Respiratory-triggered T2-weighted sequences as an alternative to the breath-hold strategy have been studied with contradictory results [16, 19, 20]. An advantage of respiratory-triggered sequences is the possibility to perform high-resolution examinations with 5 mm slice thickness which has not been possible with breath-hold sequences due to the limited breath-hold time. If one attempts to overcome this limitation of breath-hold imaging by examinations with multiple breath-holds such that the liver is examined in several stacks of slices, then parts of the liver can be missed if the patient does not meet the same position of the diaphragm in all stacks [19].

The development of iPAT allows for a substantial reduction of acquisition time, and thus breath-hold sequences with improved spatial resolution can be used. 2D navigator-based techniques, as the Prospective Acquisition

Correction (PACE) technique, known from cardiac imaging, can adapt the stacks of slices according to the respiratory position by registering the diaphragm position, so that the whole liver can be covered even if the patient does not hold his breath at the same position [21].

We compared four high-resolution T2-weighted sequences with 5 mm slice thickness and a 320×240–256 matrix for routine liver imaging: a breath-hold TSE sequence with and without iPAT and PACE (echo train length: 27, TR = 2120 ms, TE = 87 ms, 4 breath-hold cycles, iPAT factor 2, 24 reference lines), and a respiratory-triggered TSE sequence with and without iPAT (echo train length: 25, min. TR = 2680 ms, TE = 117 ms, iPAT factor 2, 24 reference lines). All images were acquired with a 12-element surface coil system dedicated to iPAT applications. A respiration belt was used for respiratory triggering. The aim was to demonstrate the feasibility of iPAT and PACE for T2-weighted liver imaging and to evaluate image quality of the different sequences.

Image examples of all sequences are shown in Fig. 20 and 21. In general, imaging with iPAT reduced the acquisition time by about 40 % without visible SNR loss. Comparing breath-hold and respiratory-triggered techniques, the latter turned out to be more robust in patients whereas no difference in image quality was observed in volunteers. An explanation for this result is that patients have more difficulties with the breath-hold period of up to 20 seconds. In conclusion, iPAT liver examinations with respiratory triggering appear to be the most robust approach for clinical routine examinations.

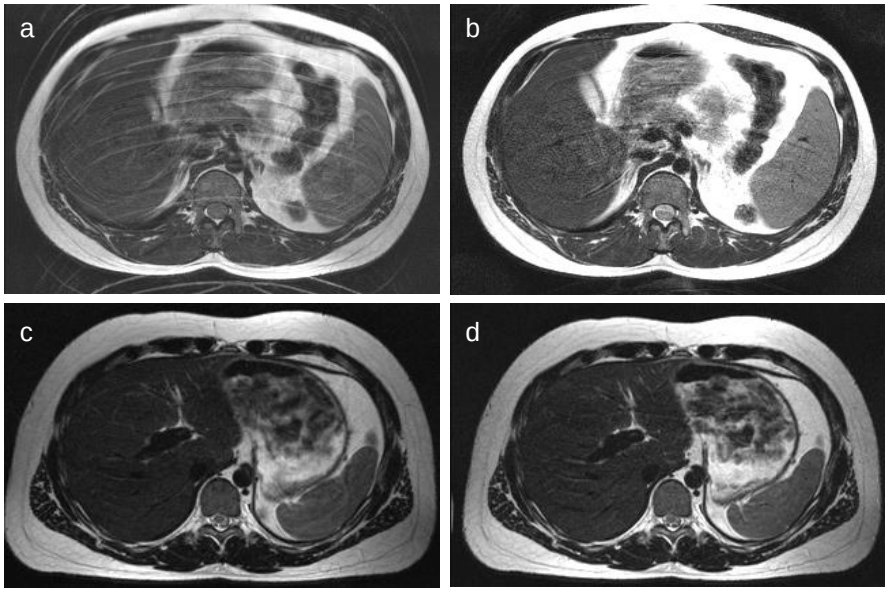

Figure 20 Examples of T2-weighted liver images: Breath-hold sequence without iPAT (a) and with iPAT (b), respiratory triggering without iPAT (c) and with iPAT (d). Note the markedly reduced artifacts in the breath-hold sequence with iPAT (b) of this subject, who had problems holding his breath. Respiratory triggering as well compensated this problem.

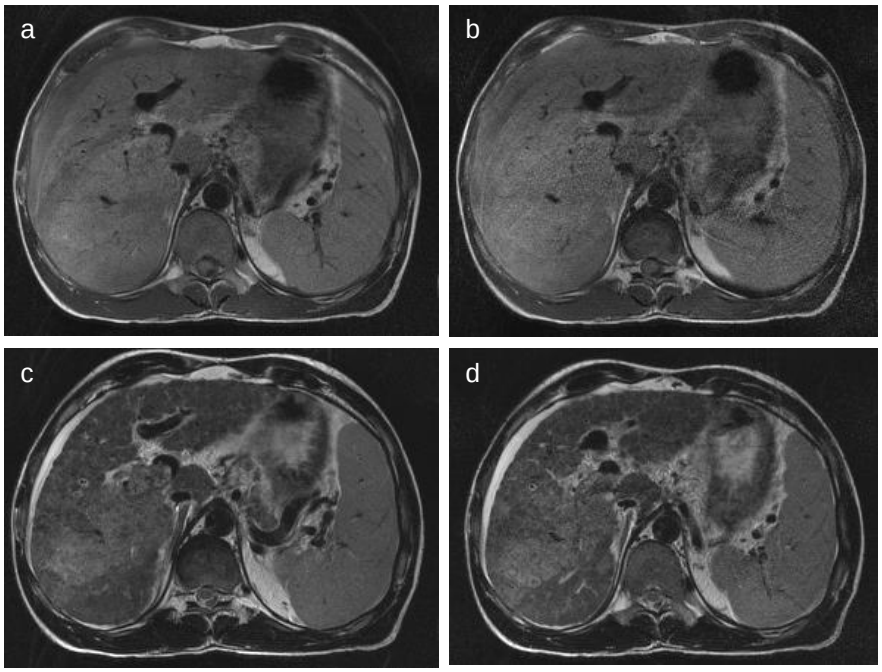

Figure 21 Examples of T2-weighted liver images: Breath-hold sequence without iPAT (a) and with iPAT (b), respiratory triggering without iPAT (c) and with iPAT (d). Respiratory triggering shows less motion artifacts and better delineation of the diffuse HCC due to better T2 contrast.

High-Resolution Renal MR Angiography

Three dimensional gadolinium-enhanced magnetic resonance angiography (3D-Gd-MRA) has gained high popularity as a non-invasive imaging alternative for grading of renal artery stenosis [22]. High accuracies of over 90 % have been reported by numerous researchers in the past five years [23]. Nevertheless, the technique is still notoriously known for overgrading high-grade renal artery stenoses and missing low-grade lesions, thereby limiting its overall clinical acceptance [24]. A recent Dutch multicenter trial presented less encouraging results with overall accuracies of only 85 % compared to DSA. In addition, no reliable data on grading of stenoses of the more distal main renal artery or segmental arteries exists, yet [25].

One major limiting factor is spatial resolution. For standard breath-hold acquisitions with bolus administration of extracellular, non-intravascular gadolinium chelates, the maximum achievable spatial resolution represents a compromise between scan time, anatomic coverage and SNR. Current imaging protocols usually obtain images with a maximum of 1.5 mm^3 isotropic resolution which still represents 5 to 7 fold less than that of digital subtraction angiography (DSA). In a renal artery with a diameter of 7–8 mm, an isotropic voxel size of at least 1 mm^3 is required for accurate depiction of a 90 % reduction in lumen diameter.

Parallel acquisition techniques allow for improvement of spatial resolution without prolonging data acquisition and are well suited for images with a high SNR such as 3D-Gd-MRA. Based on previous calculations, it is expected that voxel sizes of less than 1 mm^3 are substantially limited by SNR constraints [26]. Therefore, it was our aim to increase spatial resolution to maximum values within this range. The iPAT strategy was applied on an 8-channel Magnetom Sonata Maestro Class System in combination with a fast 3D FLASH sequence (TR = 3.79, TE = 1.3, Bandwidth = 350 Hz/pixel, flip angle = 25°). Nearly isotropic data sets with a spatial resolution of 0.8×0.8×1 mm^3 could be acquired within 23 seconds [27]. For signal reception the dedicated 12-element array coil system was used. An acceleration factor of 2 was used with 24 reference lines for auto-calibration of the coils. For data acquisition and reconstruction, the GRAPPA and SENSE algorithms were compared in terms of artifacts. To improve the contrast-to-noise ratio, the one-molar contrast agent gadobutrol (Gadovist®, Schering AG, Germany) was administered at a dose of 1.25 mmol/kg body weight with an injection rate of 2 ml/s.

In the iPAT images, SNR decreased by a factor of about 1.5 compared to the data without iPAT. This decrease in SNR could be visually noticed in the source images, however the intravascular signal was still acceptable. In the MIP images, the overall decrease in SNR was hardly detected.

The high-resolution renal 3D-Gd-MRA data sets were compared to selective x-ray angiography in more than 20 patients with renal artery stenosis ranging from 20 % luminal narrowing to occlusion. Image analysis of the isotropic data sets consisted of multiplanar reformats along the vessel axis to assess the degree of diameter reduction. In addition, reformats perpendicular to the vessel axis were performed to assess the degree of reduction of vessel area. Using multiplanar reformats the degree of stenosis was correctly assessed in 18 of 20 patients. In 2 cases, the degree of stenosis was overestimated. However, when reformats were performed in the isotropic data sets perpendicular to the vessel axis all stenoses could be correctly identified compared to x-ray angiography (Fig. 22 and 23).

One limitation is the propagation of aliasing artifacts into the center of the image. These artifacts could be theoretically avoided by extending the FOV in the left- right direction so that no aliasing occurs at all. In clinical practice however, this would mean a substantial increase in scan time, in particular in large patients. In addition, not all patients are able to put their arms over the head. Therefore some degree of aliasing into the margins of the FOV has to be accepted. Using the GRAPPA algorithm, artifacts propagating from tissue outside the FOV into the center of the image were kept at a minimum. Only slight ring-like artifacts occurred, which did not affect the image interpretation. However, when the mSENSE technique was alternatively used, these artifacts were more severe (Fig. 24).

In conclusion, high-resolution renal 3D-Gd-MRA using iPAT allows for substantial improvement of spatial resolution, thereby increasing diagnostic accuracy compared to digital subtraction angiography. Using the GRAPPA based algorithm, artifacts propagating into the center of the FOV can be kept at a minimum.

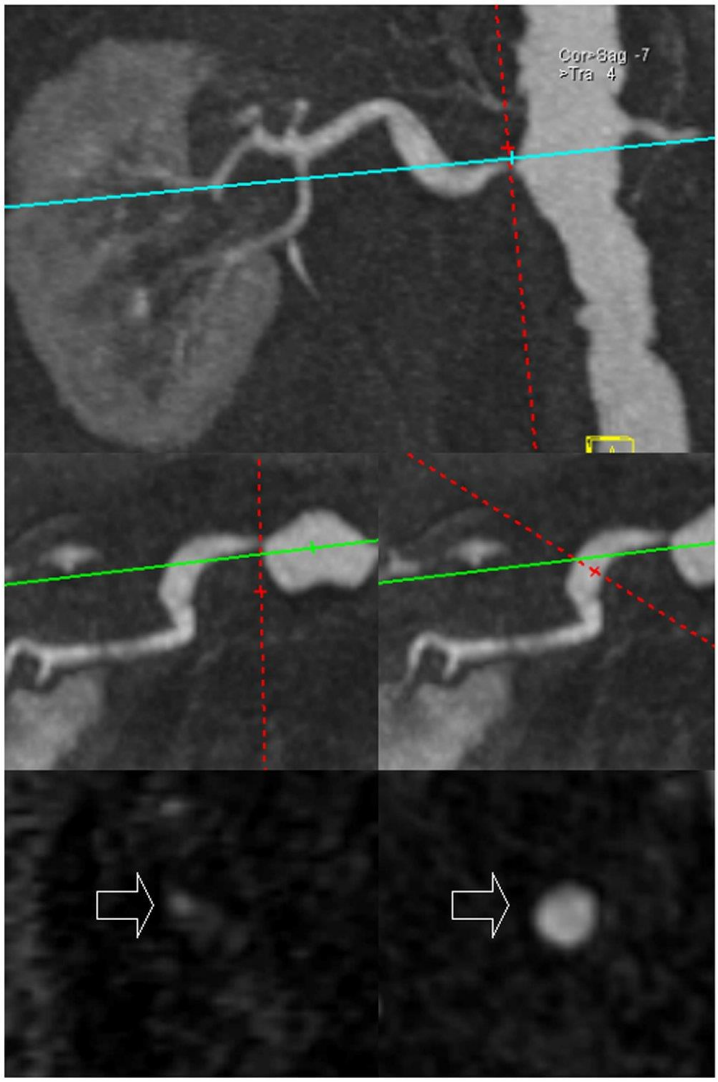

Figure 22 Multiplanar reformats of a high-resolution 3D-Gd-MRA. In the cross-sectional reformats of the vessel (lower image series) even the area of the stenotic lumen can be clearly demonstrated due to the isotropic spatial resolution.

Figure 23 Coronal MIP image of high-resolution MRA with iPAT (a) reveals excellent agreement to DSA (b). Both high-grade renal artery stenoses are seen including the residual vessel lumen. Note the absence of any major aliasing artifacts in the center of the image.

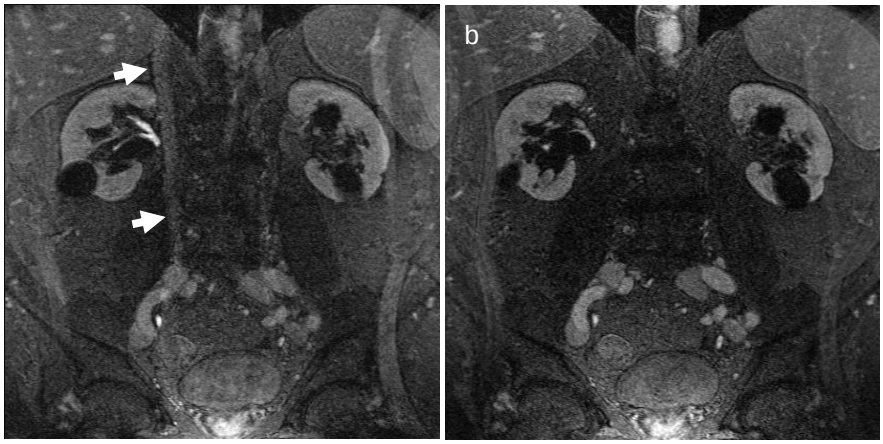

Figure 24 Comparison of propagated aliasing artifacts in the same patient using the mSENSE (a) and GRAPPA (b) algorithm. The field of view was on purpose set to only 32 cm to enforce aliasing of the arms. In the mSENSE images severe artifacts occur in the center of the image (arrows) while these artifacts are virtually absent on the GRAPPA images.

Whole-Body Imaging/Screening

Because of the recent improvements in hardware and software and the lack of ionizing radiation, magnetic resonance imaging has become a candidate for screening imaging [28]. We developed an MR examination which combines well established components including functional cardiac imaging together with myocardial perfusion imaging, imaging of the lung, brain, an overall view of liver, kidneys, spleen, and pancreas, as well as the arterial system.

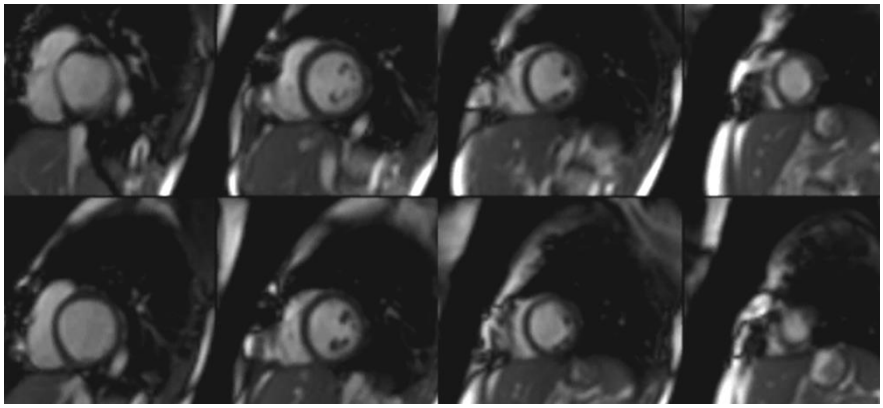

Figure 25 Single breath-hold evaluation of global cardiac function with real-time iPAT TrueFISP.

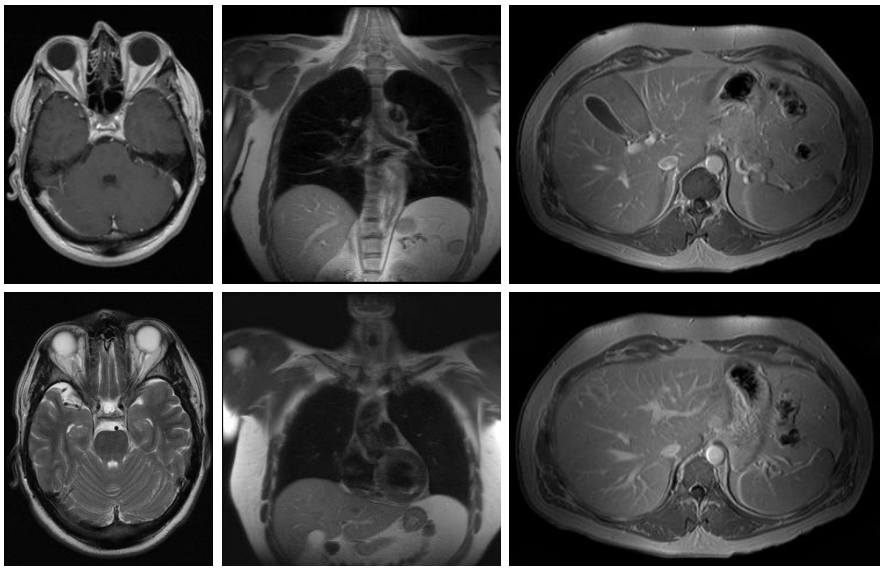

Figure 26 Imaging of the brain, lungs, and abdomen as part of the whole-body screening examination.

The whole-body examination is performed in two parts. In the first part, the patient is in a head first position; the spine array, two body arrays, and a head array are used as receiver coils. In the second part, the patient is in a feet first position; the spine array, the large FOV adapter, one or two body arrays (depending to the height of the patient), and the peripheral angio array are used as receiver coils. iPAT with an acceleration factor of two is applied for most scans of the examination including real-time TrueFISP imaging of the heart (Fig. 25), high-resolution imaging of the lung (Fig. 26) as well as dynamic cardiac perfusion MRI with TrueFISP. In addition,

Figure 27 Example of gadolinium-enhanced MR angiography as part of the whole-body screening examination. Note the excellent visualization of vessel segments down to the pedal arch. No stenoses are present.

iPAT of 3D-Gd-MRA in combination with the large FOV adapter is performed for all studies allowing a total scan time of only 62 seconds to cover the area from the thoracic aorta down to the toes at a spatial resolution of less than 1.4×1.0×1.5 mm^3 (Fig. 27).

By applying the GRAPPA algorithm with its integrated auto-calibration scan, it is possible to use flexible combinations of receiver coils with a flexible choice of iPAT directions and to move the patient table for different iPAT acquisitions. The advantage of iPAT in this kind of exam is the coverage of a large anatomic region and gain of time so that a whole-body scan can be done within 90 minutes without loss of image quality.

In the last two months twenty individuals sent by their referring physician while participating in a manager healthcare program underwent the whole-body scan in our department. All twenty individuals tolerated the MR examination well. Compared to the conventional examination techniques like ultrasound and ECG we have established a more comprehensive exam within reasonable scan time. First results of pathologic findings (scar in lung, aortic stenosis, renal artery stenosis) show good correlation with the gold standard examinations.

Conclusion

This overview on applications and ongoing studies in different areas of the body supports the current trend to use parallel imaging in the majority of clinical scan protocols. The general advantages of parallel imaging are now well established. This includes the possibility for higher spatial resolution for 3D-Gd-MRA with shorter breath-holds which improves the accuracy of this technique for grading of renal artery stenosis. The combination of time-resolved and high-resolution 3D-Gd-MRA improves the detection and differentiation of pulmonary hypertension. The use of shorter echo trains for single shot HASTE or echo planar imaging results in less image distortion and less signal decay. Initial results show benefits for EPI diffusion tensor imaging in the brain as well as detection of early infiltrates in the lung with HASTE imaging. Imaging with multiple averages in shorter acquisition times improves detection of tumors in areas with increased motion such as the larynx. Higher temporal resolution improves the accuracy of cardiac real-time techniques using SSFP sequences to measure global cardiac function within a single breath-hold.

In addition to the general benefits of parallel imaging, the iPAT methods GRAPPA and mSENSE feature some unique advantages. Artifacts in the center of coronal images resulting from aliasing of tissue outside the FOV are substantial suppressed using the GRAPPA algorithm. The iPAT algorithms with auto-calibration integrated into the individual scan are less sensitive to patient motion as other parallel imaging techniques with a single measurement of the coil sensitivity profiles at the start of the examination. In addition, the integrated auto-calibration allows a flexible combination of multiple receiver coil systems. Therefore, large anatomic coverage with various receiver coils and a flexible choice of the iPAT directions is possible. This is particularly helpful for whole-body imaging where multiple receiver coil systems are combined to scan the entire body with parallel imaging techniques. Scan time for a complete cardiovascular exam is substantially reduced while spatial and temporal resolution of the individual scans are preserved.

In conclusion, iPAT can be used to improve most clinical protocols for comprehensive morphologic and functional imaging. Depending on the specific application its main advantages are a decrease in imaging artifacts or an increase in speed, spatial, or temporal resolution.

Co-Workers on Parallel Imaging

Roger Eibel (pulmonary imaging)
Wilhelm Flatz (imaging of the larynx)
Peter Herzog (pulmonary imaging)
Armin Huber (cardiac imaging)
Wolfgang Klinger (MR technician)
Harald Kramer (whole-body imaging and screening)
Konstantin Nikolaou (cardiac imaging and pulmonary imaging)
Carola Schmid (MR technician)
Frank Stadie (MR technician)
Robert Stahl (diffusion tensor imaging)
Anja Struwe (MR technician)
Bernd J. Wintersperger (cardiac imaging)
Christoph Zech (abdominal imaging)

Acknowledgements

We would like to thank the Magnetic Resonance Development Department of Siemens Medical Systems and especially Mathias Nittka, Berthold Kiefer, and Rolf Sauter for their technical support.

References

[1] Griswold MA, Jakob PM, Heidemann RM, Nittka M, Jellus V, Wang J, Kiefer B, Haase A. Generalized autocalibrating partially parallel acquisitions (GRAPPA). Magn Reson Med 2002; 47: 1202–1210

[2] Sodickson DK, Manning WJ. Simultaneous acquisition of spatial harmonics (SMASH): fast imaging with radiofrequency coil arrays. Magn Reson Med 1997; 38: 591–603

[3] Pruessmann KP, Weiger M, Scheidegger MB, Boesiger P. SENSE: sensitivity encoding for fast MRI. Magn Reson Med 1999; 42: 952–962

[4] Basser PJ, Pierpaoli C. A simplified method to measure the diffusion tensor from seven MR images. Magn Reson Med 1998; 39: 928–934

[5] Le Bihan D, Mangin JF, Poupon C, Clark CA, Pappata S, Molko N, Chabriat H. Diffusion tensor imaging: concepts and applications. J Magn Reson Imaging 2001; 13: 534–546

[6] Keberl M, Kenn W, Hahn D. Current concepts in imaging of laryngeal and hypopharyngeal cancer. Eur Radiol. 2002; 12: 1672–1683

[7] Biederer J, Busse I, Grimm J, Reuter M, Muhle C, Freitag S, Heller M. Sensitivity of MRI in detecting alveolar Infiltrates: Experimental studies. Rofo Fortschr Geb Rontgenstr Neuen Bildgeb Verfahr. 2002; 174: 1033–1039

[8] Amundsen T, Torheim G, Kvistad KA, Waage A, Bjermer L, Nordlid KK, Johnsen H, Asberg A, Haraldseth O. Perfusion abnormalities in pulmonary embolism studied with perfusion MRI and ventilation-perfusion scintigraphy: an intra-modality and inter-modality agreement study. J Magn Reson Imaging 2002; 15: 386–394

[9] Hatabu H, Tadamura E, Prasad PV, Chen Q, Buxton R, Edelman RR. Noninvasive pulmonary perfusion imaging by STARHASTE sequence. Magn Reson Med 2000; 44: 808–812

[10] Mai VM, Hagspiel KD, Christopher JM, Do HM, Altes T, Knight-Scott J, Stith AL, Maier T, Berr SS. Perfusion imaging of the human lung using flow-sensitive alternating inversion recovery with an extra radiofrequency pulse (FAIRER). Magn Reson Imaging 1999; 17: 355–361

[11] Barkhausen J, Goyen M, Ruhm SG, Eggebrecht H, Debatin JF, Ladd ME. Assessment of ventricular function with single breath-hold real-time steady-state free precession cine MR imaging. Am J Roentgenol 2002; 178: 731–735

[12] Lee VS, Resnick D, Bundy JM, Simonetti OP, Lee PWeinreb JC. Cardiac function: MR evaluation in one breath hold with real-time true fast imaging with steady-state precession. Radiology 2002; 222: 835–842

[13] Miller S, Simonetti OP, Carr J, Kramer U, Finn JP. MR imaging of the heart with cine true fast imaging with steady-state precession: influence of spatial and temporal resolutions on left ventricular functional parameters. Radiology 2002; 223: 263–269

[14] Wintersperger BJ, Nikolaou K, Dietrich O, Rieber, J, Nittka M, Reiser MF, Schoenberg SO. Single breath-hold real-time cine MR imaging: Improved temporal resolution using generalized autocalibrating partially parallel acquisition (GRAPPA) algorithm. Eur Radiol 2003 (in press)

[15] Schreiber WG, Schmitt M, Kalden P, Mohrs OK, Kreitner KF, Thelen M. Dynamic contrast-enhanced myocardial perfusion imaging using saturation-prepared TrueFISP. J Magn Reson Imaging 2002; 16: 641–652

[16] Katayama M, Masui T, Kobayashi S, Ito T, Takahashi M, Sakahara H, Nozaki A, Kabasawa H. Fat-suppressed T2-weighted MRI of the liver: comparison of respiratory-triggered fast spin-echo, breath-hold single-shot fast spin-echo, and breath-hold fast-recovery fast spin-echo sequences. J Magn Reson Imaging 2001; 14: 439–449

[17] Gaa J, Hatabu H, Jenkins RL, Finn JP, Edelman RR. Liver masses: replacement of conventional T2-weighted spin-echo MR imaging with breath-hold MR imaging. Radiology 1996; 200: 459–464

[18] Hori M, Murakami T, Kim T, Kanematsu M, Tsuda K, Takahashi S, Takamura M, Hoshi H, Nakamura H. Single breath-hold T2-weighted MR imaging of the liver: value of single-shot fast spin-echo and multishot spin-echo echoplanar imaging. AJR Am J Roentgenol 2000; 174: 1423–1431

[19] Augui J, Vignaux O, Argaud C, Coste J, Gouya H, Legmann P. Liver: T2-weighted MR imaging with breath-hold fast-recovery optimized fast spin-echo compared with breath-hold half-Fourier and non-breath-hold respiratory-triggered fast spin-echo pulse sequences. Radiology 2002; 223: 853–859

[20] Tang Y, Yamashita Y, Namimoto T, Abe Y, Takahashi M. Liver T2-weighted MR imaging: comparison of fast and conventional half-Fourier single-shot turbo spin-echo, breath-hold turbo spin-echo, and respiratory-triggered turbo spin-echo sequences. Radiology 1997; 203: 766–772

[21] Liu YL, Riederer SJ, Rossman PJ, Grimm RC, Debbins JP, Ehman RL. A monitoring, feedback, and triggering system for reproducible breath-hold MR imaging. Magn Reson Med 1993; 30: 507–511

[22] Prince MR, Narasimham DL, Stanley JC, Chenevert TL, Williams DM, Marx MV, Cho KJ. Breath-hold gadolinium-enhanced MR angiography of the abdominal aorta and its major branches. Radiology 1995; 197: 785–792

[23] Dong Q, Schoenberg SO, Carlos RC, Neimatallah M, Cho KJ, Williams DM, Kazanjian SN, Prince MR. Diagnosis of renal vascular disease. Radiographics 1999; 19: 1535–1554

[24] Schoenberg SO, Bock M, Knopp, MV, Essig M, Laub G, Hawighorst, H, Zuna I, Kallinowski F, van Kaick G. Renal arteries: Optimization of 3D Gadolinium MR Angiography with bolus-timing independent fast multiphase acquisition in a single breath hold. Radiology 1999; 201: 667–676

[25] Schoenberg SO, Knopp MV, Londy F, Krishnan S, Zuna I, Lang N, Essig M, Hawighorst H, Maki JH, Stafford-Johnson D, Kallinowski F, Chenevert TL, Prince MR. Morphologic and functional magnetic resonance imaging of renal artery stenosis: a multireader tricenter study. J Am Soc Nephrology 2002; 13: 158–169.

[26] Heid O. The outer limits of contrast enhanced MR angio (gradient performance, resolution, speed, etc). In: Proceedings of the tenth international workshop on magnetic resonance angiography, Park City, Utah, The International MR Angio Club 1998: 75

[27] Schoenberg SO, Rieger J, Johannson LO, Dietrich O, Bock M, Prince MR, Reiser MF. Diagnosis of renal artery stenosis with magnetic resonance angiography – update 2003. Nephrol Dial Transplant 2003, 18: 1252–1256

[28] Goyen M, Herborn CU, Kroger K, Lauenstein TC, Debatin JF, Ruehm SG. Detection of atherosclerosis: systemic imaging for systemic disease with whole-body three-dimensional MR angiography–initial experience. Radiology. 2003; 227: 277–282